



OPEN ACCESS

EDITED BY

Pedro Berraondo,
Cima Universidad de Navarra, Spain

REVIEWED BY

Fabian Benencia,
Ohio University, United States
Tahir Bashir Dar,
Cedars Sinai Medical Center, United States

*CORRESPONDENCE

JunRong Du

✉ dujr_1@163.com

Cheng Peng

✉ pengchengchengdu@126.com

Fu Peng

✉ fujing126@yeah.net

RECEIVED 22 November 2024

ACCEPTED 20 March 2025

PUBLISHED 14 April 2025

CITATION

Li S, Wang L, Han M, Fan H, Tang H, Gao H, Li G, Xu Z, Zhou Z, Du J, Peng C and Peng F (2025) Combination of Sodium Butyrate and Immunotherapy in Glioma: regulation of immunologically hot and cold tumors via gut microbiota and metabolites. *Front. Immunol.* 16:1532528. doi: 10.3389/fimmu.2025.1532528

COPYRIGHT

© 2025 Li, Wang, Han, Fan, Tang, Gao, Li, Xu, Zhou, Du, Peng and Peng. This is an open-access article distributed under the terms of the [Creative Commons Attribution License \(CC BY\)](https://creativecommons.org/licenses/by/4.0/). The use, distribution or reproduction in other forums is permitted, provided the original author(s) and the copyright owner(s) are credited and that the original publication in this journal is cited, in accordance with accepted academic practice. No use, distribution or reproduction is permitted which does not comply with these terms.

Combination of Sodium Butyrate and Immunotherapy in Glioma: regulation of immunologically hot and cold tumors via gut microbiota and metabolites

Sui Li^{1,2}, Li Wang³, MingYu Han¹, Huali Fan¹, Hailin Tang⁴, Huile Gao¹, Guobo Li¹, Zheng Xu⁵, Zhaokai Zhou⁶, JunRong Du^{1*}, Cheng Peng^{2*} and Fu Peng^{1,7*}

¹West China School of Pharmacy, Sichuan University, Chengdu, China, ²State Key Laboratory of Southwestern Chinese Medicine Resources, School of Pharmacy, Chengdu University of Traditional Chinese Medicine, Chengdu, China, ³Bioinformatics Department, Jiangsu Sanshu Biotechnology Co., Ltd., Nantong, China, ⁴State Key Laboratory of Oncology in South China, Guangdong Provincial Clinical Research Center for Cancer, Sun Yat-Sen University Cancer Center, Guangdong, China, ⁵State Key Laboratory of Biotherapy, West China Hospital, Sichuan University, Chengdu, China, ⁶Department of Urology, The First Affiliated Hospital of Zhengzhou University, Department of Clinical Medicine, Zhengzhou University, Henan, China, ⁷Key Laboratory of Drug-Targeting and Drug Delivery System of the Education Ministry, Sichuan Engineering Laboratory for Plant-Sourced Drug and Sichuan Research Center for Drug Precision Industrial Technology, West China School of Pharmacy, Sichuan University, Chengdu, China

Background: Recent studies have highlighted the importance of cross-talk along the gut-brain axis in regulating inflammatory nociception, inflammatory responses, and immune homeostasis. The gut microbiota, particularly its bacterial composition, plays a crucial role in the development and function of the immune system. Moreover, metabolites produced by the gut microbiota can significantly impact both systemic immune responses and central nervous system (CNS) immunity. Sodium butyrate is a key metabolite produced by the gut microbiota and, as a histone deacetylase inhibitor, can enhance the anti-tumor immunity of cytotoxic CD8⁺ T cells. However, it remains unclear whether sodium butyrate treatment can enhance the efficacy of PD-1 blockade in glioma therapy. In this research, the effect and underlying mechanism of combination of gut microbiota metabolites and anti-mouse PD-1 mAb on glioma has been investigated.

Methods: RNA-seq assay in glioma cell and biomedical databases, including ONCOMINE, GEPIA and TCGA were incorporated. Subsequently, the inhibitory effect of sodium butyrate on glioma cells and its related mechanisms were assessed through Counting Kit-8 (CCK-8), Flow Cytometry, Western blot (WB), reverse transcription-quantitative polymerase chain reaction (RT-qPCR), and other *in vitro* experiments. *In vitro*, an orthotopic mouse glioma model was established. MRI imaging, Immunohistochemistry, and Immune cell flow cytometry were used to investigate the therapeutic effects of combined sodium butyrate and PD-1 inhibitor treatment on glioma-bearing mice.

Results: We discovered that deacetylation-associated gene expression is significantly increased in glioma patients and affects patient survival time.

Moreover, we found sodium butyrate promoted glioma cell apoptosis, disrupted the cell cycle, and inhibited tumor growth. Additionally, sodium butyrate may upregulate PD-L1 expression in glioma cells by modulating the PI3K/AKT pathway. The experimental results demonstrated that this combination therapy significantly reduced tumor volume and prolonged survival in an orthotopic murine glioma model. Moreover, combination therapy led to an increase in the proportion of probiotic bacteria in the mouse gut microbiota, resulting in elevated levels of antitumor metabolites and a decrease in metabolites that affect immune cell function.

KEYWORDS

anti-tumor immunity, gut microbiota and metabolites, glioma, sodium butyrate, PD-1/PD-L1, PI3K/Akt signaling pathway

1 Introduction

Glioma is considered one of the most malignant tumors affecting the central nervous system and has high mortality and recurrence rates (1–3). Although PD-L1 is generally considered an immunosuppressive molecule, its expression may not always signify tumor immune evasion and could instead reflect an ongoing antitumor immune response (4). In glioma, which is classified as a “cold” tumor with fewer CD3 T cells, a greater frequency of myeloid cells (monocytes, macrophages, and microglia), and lower expression of PD-L1 and PD-1-expressing TILs (5–7), a phase III clinical trial of PD-1 for glioma revealed an overall treatment response rate of only 8% and did not significantly prolong the overall survival of glioma patients (8). Therefore, enhancing PD-L1 expression to increase T cell infiltration may offer a potential strategy for converting gliomas from ‘cold’ tumors to ‘hot’ tumors.

Recent studies have established a connection between the gut microbiome and the efficacy of immune checkpoint inhibitors (9–11). The potential mechanisms through which the gut microbiota mediates anti-tumor immunity involve the activation of T cell responses specific to microbial antigens. These responses either support tumor-specific immune activation or may cross-react with tumor-specific antigens (12, 13). However, it remains unclear how metabolites produced by the gut microbiota regulate anti-tumor immunity, and whether they can modulate tumor-infiltrating T cell responses in glioma.

In this study, we report that the sodium butyrate acted as gut microbiota metabolites to suppress glioma cell growth while increasing PD-L1 expression in glioma cells by activating the PI3K/AKT pathway. When combined with an anti-mouse PD-1 mAb, sodium butyrate resulted in tumor regression and an increased antitumor immune response in an orthotopic murine glioma model. Mechanistically, combination therapy enhanced immune cytokine levels and T-cell infiltration while also influencing the gut microbiota and its metabolites in mice.

2 Materials and methods

2.1 Cell culture

The human cell line U251 and the murine cell line GL261 were purchased from Zhong Qiao Xin Zhou Biotechnology (Shanghai, China). All cell lines were authenticated using STR profiling and cultured in DMEM (Gibco, MA, United States) supplemented with 10% fetal bovine serum (Gibco, MA, United States) and 1% penicillin/streptomycin (Invitrogen, MA, United States).

2.2 Sodium butyrate

Sodium butyrate was purchased from Sigma. Aliquots of DMSO-reconstituted Sodium butyrate were stored at -80°C . For *in vitro* studies, stocks were diluted to the final concentration immediately prior to use. For *in vivo* use, sodium butyrate was dissolved and sonicated in sterile PBS.

2.3 CCK-8 assay

Cells were seeded into 96-well plates (1×10^5 cells/well) and cultured until cell attachment. After sodium butyrate administration for 48 h, 10 μL of Cell Counting Kit-8 (CCK-8) reagent (Dojindo, Japan) was added to each well, and the plates were incubated for 1 h. The absorbance of each well was measured at 450 nm using a 96-well plate reader (Thermo Fisher Scientific, USA).

2.4 Flow cytometry analyses

After the administration of sodium butyrate and 48 hours of incubation, apoptosis and the cell cycle distribution were analyzed

using flow cytometry. For cell apoptosis analysis, the cells were collected and stained with Annexin V-FITC and propidium iodide (PI) in the dark following the procedure of the Apoptosis Detection Kit from Solarbio (China). For cell cycle analysis, the cells were collected and fixed in 70% ethanol for 2 hours at 4°C. Subsequently, the cells were stained with RNase and PI reagent in the dark following the protocol of the Cell Cycle Analysis Kit from Beyotime (China). After incubation, the cells were analyzed using a flow cytometer (FACSCelesta, BD, USA).

The tumor tissues were processed mechanically to obtain single-cell suspensions, and the cell concentration was adjusted to 10^6 cells/mL using PBS. For each tissue, two flow cytometry tubes were prepared. To each tube, 100 μ L of the single-cell suspension was added along with the fluorochrome-conjugated mAbs specific for mouse CD3, CD4, CD8, and Tregs (BD Pharmingen, USA). Tumor A: CD3, CD4, CD8, PD-L1, B220, Live-dead. Tumor B: CD4, CD25, Live-dead. The tubes were incubated at 4°C in the dark for 30 minutes. After incubation, tube A was washed with PBS, then resuspended in 400 μ L of PBS and analyzed using the FACSCanto Flow Cytometer (BD Biosciences). Tube B was subjected to fixation and permeabilization following the procedure outlined in the reagents manual. Following fixation and permeabilization, 1 μ g each of FoxP3 and IFN- γ antibodies (both from BD Pharmingen) were added, mixed, and incubated at 4°C in the dark for 30 minutes. After incubation, 400 μ L of PBS was added to re-suspend the cells, and immediate analysis was conducted using the FACSCanto Flow Cytometer (BD Biosciences). The data were acquired using a FACSCanto Flow Cytometer (BD Biosciences) and analyzed using FlowJo software (TreeStar, V7.6.5 for Windows).

2.5 Mouse models and drug administration

7 week male C57BL/6 mice (20–22g) were purchased from Beijing Huhukang Laboratory Animal Company (Beijing, China). For the *in vivo* study, mice were orthotopically implanted with 1×10^5 GL261 glioma cells. Assessment of tumor growth and survival was conducted after daily intraperitoneal administration of 1.2 g/kg sodium butyrate (Sigma, USA), either alone or in combination with 100 μ g of PD-1 blocking antibody from BioXCell twice weekly, for a total of 4 weeks, starting on the seventh day after GL261 inoculation. The treatment control group received sterile PBS. The mice were euthanized 28 days after inoculation. All animal experiments adhered to the regulations of the ethics committee of the Experimental Animal Administration of Sichuan University.

2.6 Magnetic resonance imaging

Cerebral magnetic resonance imaging (MRI) was conducted on a small animal 7 T MRI scanner (Time Medical, Shanghai, China) *in vivo*. Every mouse was given anesthesia with 2% isoflurane administered through inhalation. Imaging was performed using a

2D T2-weighted sequence in the axial orientation. Tumor volumes were calculated using ITK-SNAP program.

2.7 Western blot

Total proteins were extracted with RIPA buffer (Beyotime, Shanghai, China) according to the manufacturer's instructions. The lysates were then subjected to SDS-PAGE and transferred to a PVDF membrane (Bio-Rad, CA, United States). Primary antibody incubation was carried out overnight at 4°C. Antibodies against p-PI3K, PI3K, p-AKT, AKT, survivin, Cyclin A2, Cyclin B1, cdc2, p-cdc2, cdc25C, HDAC1, HDAC2, HDAC3 and HDAC6 were purchased from Cell Signaling Technology (Shanghai, China). Subsequently, the immunoblots were incubated with the appropriate secondary antibody, detected using ECL Plus Reagent (Beyotime, Shanghai, China) and quantified using ImageJ software.

2.8 Quantitative real-time PCR

Cells or tissues were lysed using TRIzol from Invitrogen (Thermo Fisher Scientific, MA, United States). RNA was isolated from the samples using a standard phenol-chloroform separation protocol, and cDNA was generated with an iScript kit from Bio-Rad. Expression levels were assessed by quantitative real-time PCR using the SYBR Green platform on a Bio-Rad CFX96 system. Real-time polymerase chain reaction (PCR) was conducted following previous methods, and the data were processed using the $2^{-\Delta\Delta CT}$ method (14). 18S ribosomal RNA was used as the reference gene in all experiments. Primers were designed using NCBI-Blast listed in [Supplementary Table S1](#).

2.9 Histological and immunohistochemical analyses

Paraffin-embedded tissues were cut into 3- μ m-thick sections. Hematoxylin and eosin (HE) staining was carried out following standard histological protocols. For immunohistochemistry (IHC), the slides were incubated with the following primary antibodies from Abcam (Cambridge, United Kingdom) after blocking: Ki-67 (ab16667), CD4 (ab133616), and CD8 (ab217344). Quantification of the IHC results was performed by counting the number of immunostaining-positive cells using Image-Pro Plus software.

2.10 Gene expression profiling interactive and molecular docking analysis

The mRNA sequencing data of the HDAC family together with its corresponding clinical information of glioma patients were retrieved from GEPIA (<http://gepia2.cancer-pku.cn/>), a web-based interactive tool providing comprehensive and customizable

analyses with The Cancer Genome Atlas (TCGA) and Genotype-Tissue Expression Project (GTEx) RNA sequencing data as resources.

To improve the prediction of the relationship between Sodium butyrate and PI3K/AKT and HDAC related genes in the protein-protein interaction (PPI) analysis, we performed molecular association prediction. First, we obtained the structure of the gene from the Protein Data Bank (PDB) (<http://www.rcsb.org>) and acquired the 3D structure of Sodium butyrate from the PubChem database (<https://pubchem.ncbi.nlm.nih.gov/>). Next, we removed the hydrogen and ligands and dehydrated the hub gene proteins using the PyMOL 1.7.x software (<http://www.pymol.org/>). The AutoDock Tools 1.5.6 software (<https://autodock.scripps.edu/>) was used to convert the file to the PDBQT format. The PyMOL software was used to visualize the docking results.

2.11 RNA sequencing and single-cell transcriptomic analysis

The cells were incubated with sodium butyrate for 48 h, after which total RNA was isolated using TRIzol reagent (Invitrogen). Subsequently, RNA sequencing (RNAseq) was performed using a commercially available service (service ID# F18FTSSCWLJ1284, BGI, Huada Gene, Wuhan, China). In brief, total RNA was fragmented into short fragments, and mRNA was enriched using oligo (dT) magnetic beads. This was followed by cDNA synthesis, and the double-stranded cDNA was purified and enriched through PCR amplification. The library products were then sequenced using BGISEQ-500. For the data analysis, KEGG pathway and GO bioinformatics analyses were conducted by BGI utilizing the Dr. TOM approach, an in-house customized data mining system of BGI. The altered (upregulated or downregulated) expression of genes is presented as \log_2FC , representing the log-transformed fold change ($\log_2FC = \log_2[B] - \log_2[A]$, where A and B represent the gene expression values under different treatment conditions). Single-cell sequencing data of orthotopic glioma in mice was downloaded from the GEO database (GSE246154) and analyzed using the R Programming Language.

2.12 Gut microbial 16S RNA sequencing and metabolite analysis

Fecal genomic DNA was extracted using a fecal DNA extraction kit (TIANGEN, Beijing, China) following the manufacturer's instructions. We weighed 25 mg of the fecal into a centrifuge tube and added 400 μ L of a methanol/acetonitrile mixture along with magnetic beads for sample disruption. The mixture was centrifuged at 25,000 rpm for 2 minutes and set aside for later use. A mixed standard solution of seven SCFAs was prepared and serially diluted (CAL1-CAL12). A 20 μ L aliquot of the sample and 60 μ L of the standard solution were mixed with 60 μ L of cold methanol/acetonitrile (2:1), vortexed for 5 minutes, and then incubated at

-20°C for 4 hours. The mixture was centrifuged at 20,000 g at 4°C for 15 minutes, and 40 μ L of the supernatant was transferred to an EP tube. To the EP tube containing 40 μ L of the supernatant, we added 20 μ L of 200 mM 3-NPH (solvent: 50% acetonitrile) and 20 μ L of a 120 mM EDC-6% pyridine mixture (solvent: 50% acetonitrile). The reaction was incubated in a metal bath at 40°C with shaking for 30 minutes, then cooled to room temperature on ice and briefly centrifuged. After derivatization, 80 μ L of 1000 Da internal standard (solvent: 10% acetonitrile) was added and mixed well. In a filtration plate, 90 μ L of water and 90 μ L of the derivatized sample were added. The mixture was centrifuged at 3,000 g at 4°C for 5 minutes. The filtered supernatant (90 μ L) was transferred to a new 96-well plate, and 10 μ L was injected for LC-MS/MS (Waters I-Class system coupled with an AB Sciex 6500 mass spectrometer). MRM transitions (ion pairs) were automatically identified and integrated using default parameters in MultiQuant software (SCIEX, USA), with manual verification to ensure accuracy. The concentration of short-chain fatty acids (ng/mg) was calculated using the formula: FACS Concentration (ng/mg) = $(C \cdot V) / M$, where C is the concentration of the target analyte (ng/mL), V is the volume of the extracted sample (μ L), and M is the weight of the sample (mg).

The near-full-length 16S rRNA genes were amplified using the 27F/1390R primers. Subsequently, the constructed library was sequenced on the PacBio Sequel platform. The high-quality reads obtained were analyzed using QIIME software. The qualified sequences were then clustered into operational taxonomic units (OTUs) at 97% similarity. Metabolic extracts from fecal samples were analyzed by gas chromatography–mass spectrometry (GC–MS) based on a previous research protocol (15). All the analyses were conducted using BMKCloud (www.biocloud.net).

2.13 Statistical analysis

The values presented in the study represent the mean \pm SEM of at least three independent experiments. All the statistical analyses were conducted using SPSS 25.0 and GraphPad Prism 5.0 software. The log-rank test was used to analyze Kaplan–Meier survival curves. For comparisons between two groups, two-tailed Student's t tests were used. Comparisons among multiple groups were performed using one-way analysis of variance (ANOVA), followed by the least significant difference (LSD) *post hoc* test. Differences with a *p* value less than 0.05 were considered to indicate statistical significance.

3 Results

3.1 Sodium butyrate inhibits glioma cell proliferation and promotes U251 cell apoptosis

To investigate the effect of sodium butyrate on the growth of glioma, U251 and GL261 glioma cells were exposed to various

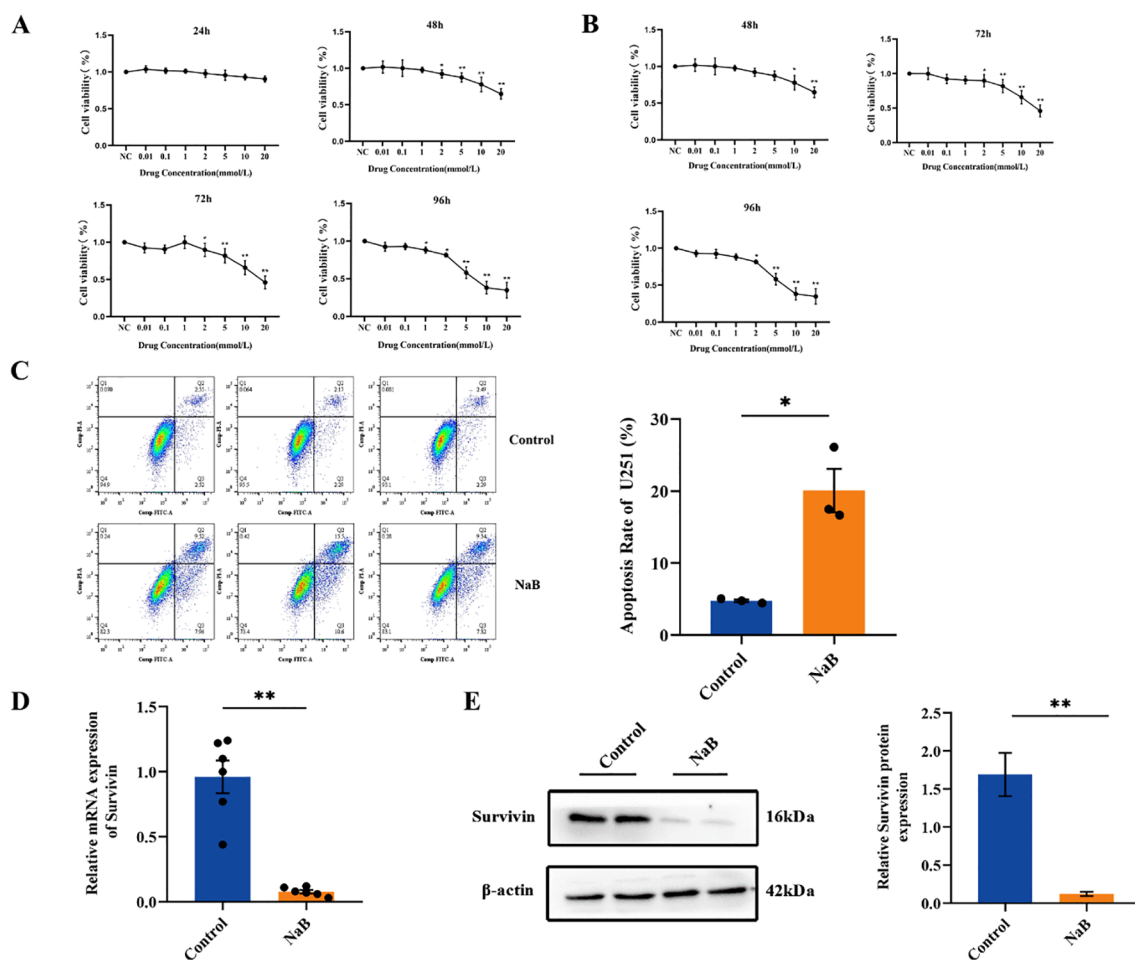


FIGURE 1

Sodium butyrate inhibits glioma cell proliferation and promotes U251 cell apoptosis. (A) U251 and (B) GL261 glioma cell viability was examined using the CCK-8 assay. The data are expressed as the mean \pm SEM of three independent experiments. One-way ANOVA was used for statistical analysis. Compared with the control group, * $p < 0.05$, ** $p < 0.01$. (C) U251 cells were treated with 7 mM sodium butyrate for 48 h, followed by flow cytometry analysis to determine the percentage of Annexin V-positive apoptotic cells. (D) The mRNA levels of Survivin in U251 cells. (E) Results of the statistical analysis of Survivin protein levels in U251 cells. The data are presented as the means \pm SDs of three independent replicates. Two-tailed, unpaired Student's t test was used for statistical analysis. Compared with the control group, * $p < 0.05$, ** $p < 0.01$.

concentrations of sodium butyrate for 24, 48, 72 or 96 h. The viability of U251 and GL261 cells was determined using CCK-8 assay. As shown in Figures 1A, B, exposure to sodium butyrate led to a significant increase in the cytotoxicity toward these glioma cells in a dose- and time-dependent manner. Notably, U251 glioma cells were more sensitive to sodium butyrate than GL261 cells. Subsequently, flow cytometry with Annexin V/PI staining was performed to examine whether sodium butyrate induces apoptosis in U251 cells. After 48 hours of exposure to sodium butyrate, the percentage of apoptotic (Annexin V-positive) U251 cells significantly increased (Figure 1C). As Survivin (also known as BIRC5) is known to play a crucial role in inhibiting tumor cell apoptosis (16), researchers have further examined the effect of sodium butyrate on Survivin. Consistent with the results for apoptosis, sodium butyrate treatment also led to a reduction in Survivin, as evidenced by decreased mRNA and protein expression of Survivin (Figures 1D, E) compared with that in the control group.

3.2 Treatment with sodium butyrate alters genome-wide gene expression in U251 cells

To gain a deeper understanding of the mechanism underlying the treatment of glioma cells with the histone deacetylase inhibitor sodium butyrate, an RNA-seq assay was performed to profile genome-wide gene expression changes in U251 cells after treatment with sodium butyrate for 48 hours. After analyzing the data, differentially expressed genes (DEGs) between the control and sodium butyrate-treated (NaB) groups were identified based on the criteria of a $|\log_2FC| \geq 2$ and a Q value ≤ 0.05 . Among these DEGs, 2022 were upregulated, and 1367 were downregulated (Figures 2A, B). KEGG analysis revealed that the most significantly altered pathways involved the cell cycle and DNA replication (Figure 2C). Additionally, significantly upregulated DEGs were enriched in the Rap1 signaling pathway, MAPK signaling pathway, and PI3K-AKT signaling pathway (Figure 2D).

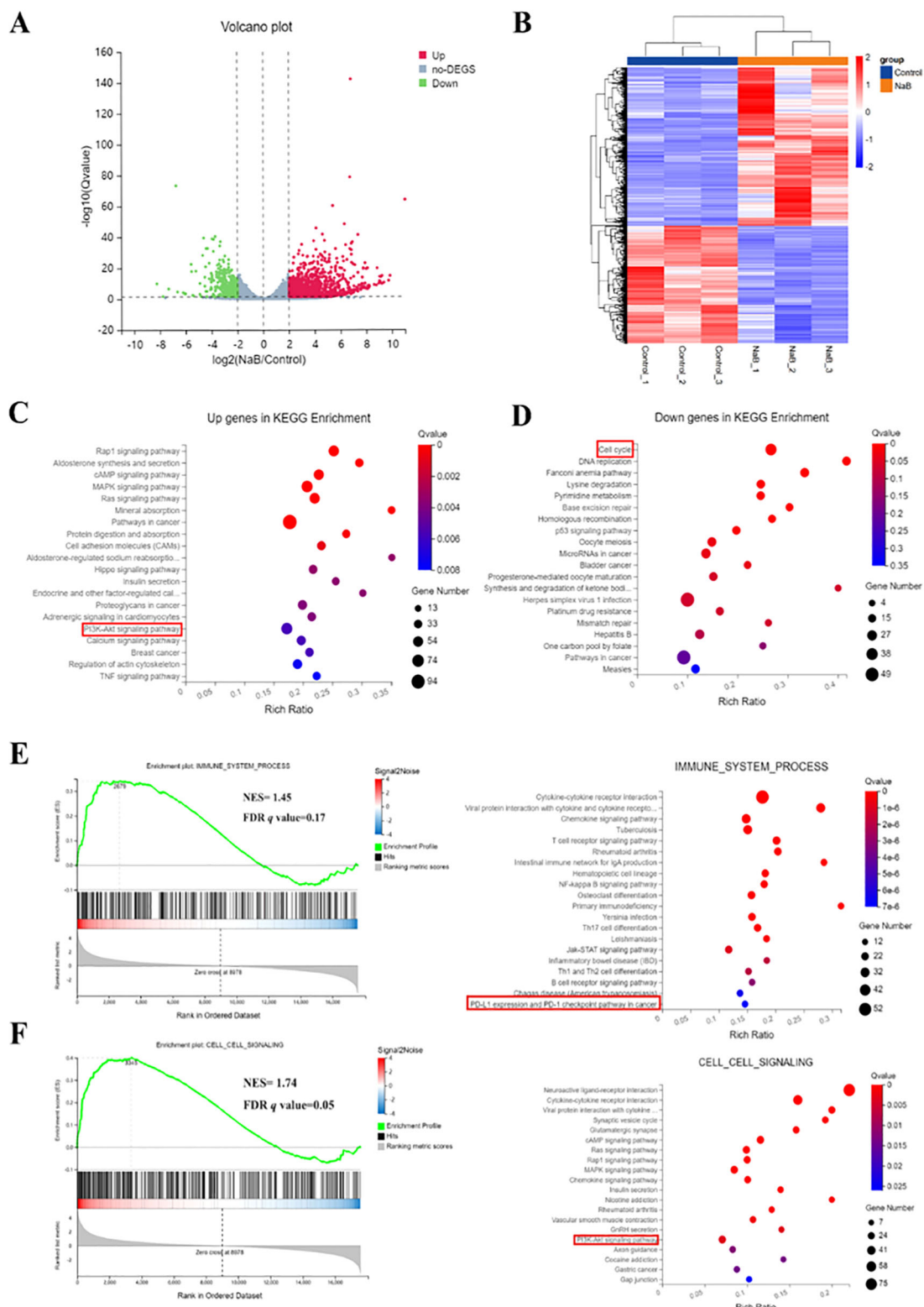


FIGURE 2 Treatment with sodium butyrate alters genome-wide gene expression in U251 cells. Volcano plot (A) and heatmap (B) of DEGs between control and NaB-treated U251 cells. (C, D) Bubble plot showing the enrichment of upregulated and downregulated genes. (E, F) Enrichment map of GSEA and KEGG pathways associated with upregulated and downregulated genes. NES, Normalized enrichment score; FDR, False positive detection rate. n=3.

Furthermore, the combined GSEA and KEGG analysis revealed that significantly downregulated or upregulated transcripts were involved in the immune system and cell signaling pathways, including PD-L1 expression, the PD-1 checkpoint pathway in cancer, and the PI3K-AKT signaling pathway (Figures 2E, F). Previous research has indicated that inducing Akt activity increases the protein expression of PD-L1, while inhibiting PI3K reduces PD-L1 protein expression in glioma cells (17). Therefore, the RNA-seq results suggest that sodium butyrate treatment affects a series of signaling pathways involved in cell cycle regulation and regulates the PI3K/AKT signaling pathway to impact the immune system of U251 cells.

3.3 Treatment with sodium butyrate blocks the U251 cell cycle

RNA-seq analysis revealed that NaB treatment significantly inhibited G2/M phase-related genes in U251 cells. The G2/M phase of the cell cycle is controlled by cell cycle protein-dependent kinases (CDKs) and cell cycle proteins of the cyclin family (18). CDC2, also known as CDK1, was the first cell cycle protein-dependent protein kinase discovered, and phosphorylated CDC2 plays a crucial role in cell cycle progression (19). CDC25C is a protease responsible for activating CDC2 through dephosphorylation and plays a key role in the regulation of mitosis (20). Cyclin B (CCNB) is essential for initiating mitosis at the G2/M checkpoint, while cyclin A (CCNA) is required for both the S and M phases of the cell cycle (21). Cyclin A2 (CCNA2) and cyclin B1 (cyclin B1, CCNB1) interact with CDC2 in cell cycle regulation, and the formation of the CDC2/cyclinB1 complex is necessary for transitioning cells from G2 to M phase (22).

To further verify the effect of NaB on the U251 cell cycle and related pathway proteins, we used PI staining to detect the cell cycle distribution of NaB-treated U251 cells. qPCR and Western blotting were used to detect the mRNA and protein levels of CDC2, CDC25C, CCNA2 and CCNB1, respectively, in U251 cells. The PI staining results demonstrated that NaB blocked U251 cells in the G2/M phase (Figure 3A, $p < 0.05$).

Furthermore, compared with those in the control group, the mRNA and protein levels of CDC2, CDC25C, CCNA2, and CCNB1 were significantly lower in the NaB-treated group (Figures 3B, C, $p < 0.05$), with the most significant reduction observed in the protein expression level of CCNA2 (Figure 3C, $p < 0.01$). These experimental results indicated that NaB significantly inhibited the cycle progression of U251 cells by downregulating the expression of cell cycle-related proteins and arresting them in the G2/M phase, which was consistent with the RNA-seq results.

3.4 Histone deacetylase expression upregulate in GBM clinical database and prolong glioma patients survival time

Besides the U251 cell RNA-seq assay results, we also search RNA-Seq data from the UALCAN database to explore the role of

HDAC and PI3K/AKT genes in the context of glioma. The mRNA expression of HDAC1, HDAC2, HDAC3, HDAC6 and PI3K/AKT1 was analyzed in GBM and low grade glioma tissues. The mRNA expression levels of HDAC1, HDAC2 and AKT1 were relatively high in glioma (Figure 4A, $p < 0.05$), while those of HDAC3 and HDAC6 have no significant difference between glioma and normal tissues (Supplementary Figure S1, $p > 0.05$). The overall survival time of glioma patients with low HDAC1, HDAC3 and AKT1 expression is better (Figure 4B, $p < 0.05$). Taken together, HDAC1 is considered as core gene in glioma.

According to the KEGG analysis, the critical pathway gene is AKT. Also, sodium butyrate act as HDACi in this study. Molecular docking showed a strong binding effect. The binding affinities of sodium butyrate to AKT (4EJN), PI3K (7jwz) and HDAC (7sme) were -4.13, -6.27 and -3.65 kcal/mol (Figure 4C). In addition, a coupling fraction of less than 0 kcal/mol indicates that the component can spontaneously bind to the target, less than -1.20 kcal/mol indicates a good affinity coupling, and less than -7 kcal/mol is considered as strong affinity coupling (2). The results indicated a good binding activity between NaB and the critical genes.

3.5 Sodium butyrate acts as a histone deacetylase inhibitor to upregulate PD-L1 protein levels in U251 cells through activation of the PI3K/AKT signaling pathway

PD-1 and PD-L1 play crucial roles in suppressing immune responses and promoting self-tolerance by modulating T-cell activity, activating the apoptosis of antigen-specific T cells, and inhibiting the apoptosis of regulatory T cells (23). High levels of PD-L1 protein expression have been observed in most human cancers (24), including glioma (17). The expression of PD-L1 in the cancer microenvironment is regulated by multiple cytokines, such as IFN- γ (25) and IL-10 (26), and is also influenced by abnormal signaling pathways (27–29). The RNA-seq results in our study indicated that sodium butyrate treatment activated the PI3K/AKT signaling pathway in U251 cells (Figure 2C), and GSEA revealed that the differentially expressed genes were involved in PD-L1 expression and the PD-1 checkpoint pathway in cancer (Figure 2E). Based on these findings, we assessed the activation of the PI3K/AKT pathway and PD-L1 expression in U251 cells treated with sodium butyrate. As shown in Figure 4A, sodium butyrate treatment upregulated the protein levels of p-PI3K and p-AKT in U251 cells compared to those in the control group ($p < 0.05$). Additionally, sodium butyrate treatment significantly upregulated the protein level of PD-L1 in U251 cells (Figure 5B, $p < 0.05$). These results were consistent with the RNA-seq analysis.

Furthermore, HDAC inhibitors (HDACs) are known to induce apoptosis and cell cycle arrest, promote cell differentiation, and inhibit angiogenesis in tumor cells (30). Recent studies have shown that HDACs play important roles in tumor immune escape and drug resistance (31). Sodium butyrate, a class I HDAC inhibitor, has been widely used to study the role of histone acetylation in chromatin structure and function (32). Based on the RNA-seq results of U251 cells

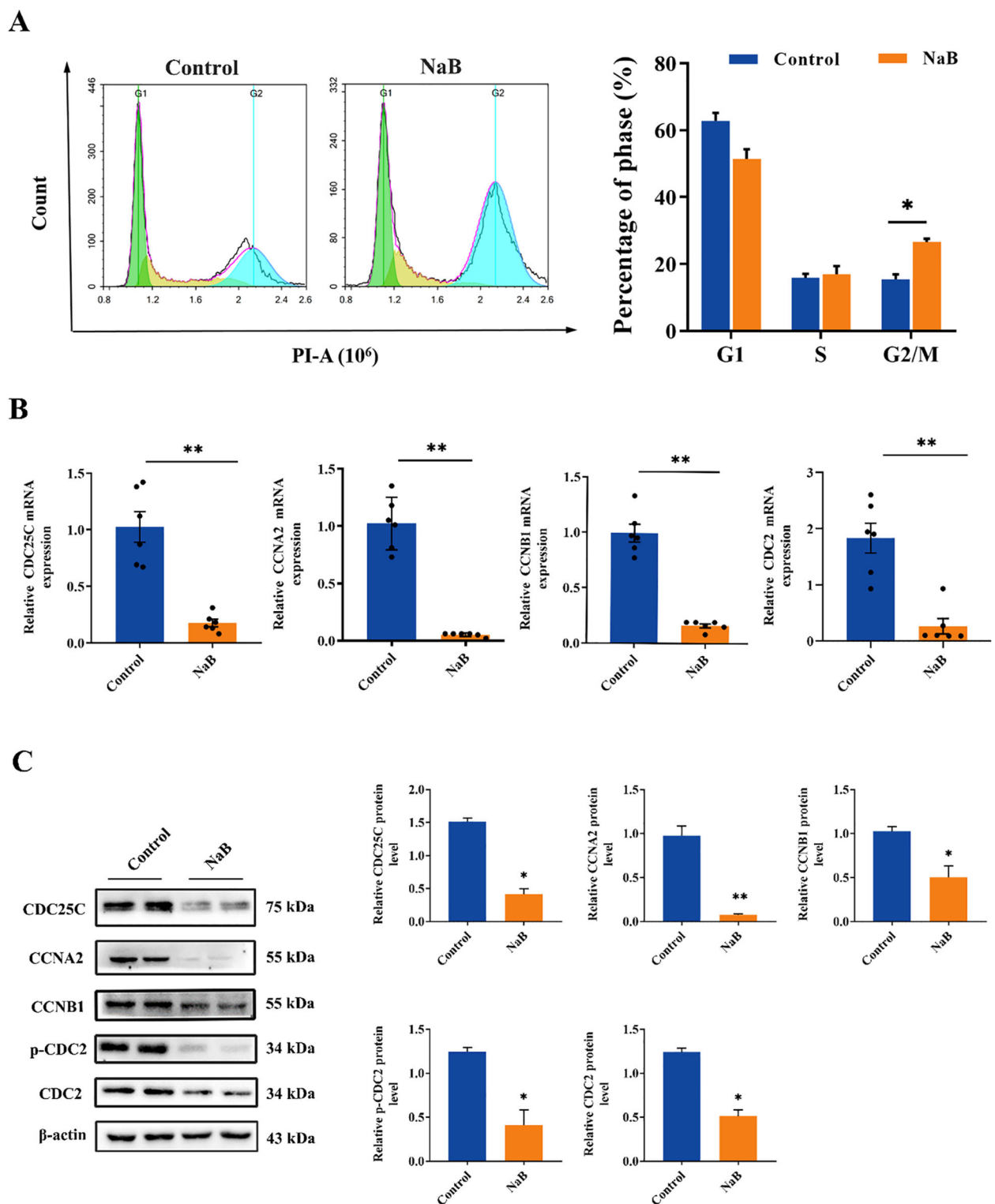


FIGURE 3

Treatment with sodium butyrate blocks the U251 cell cycle. (A) PI assay U251 cell cycle flow and statistical plot. (B) The mRNA levels of CDC25C, CCNA2, CCNB1 and CDC2 in U251 cells. (C) The protein levels of CDC25C, CCNA2, CCNB1, p-CDC2 and CDC2 in U251 cells. The data are expressed as the mean ± SEM of three independent experiments. Two-tailed, unpaired Student's t test was used for statistical analysis. Compared with the control group, * $p < 0.05$, ** $p < 0.01$.

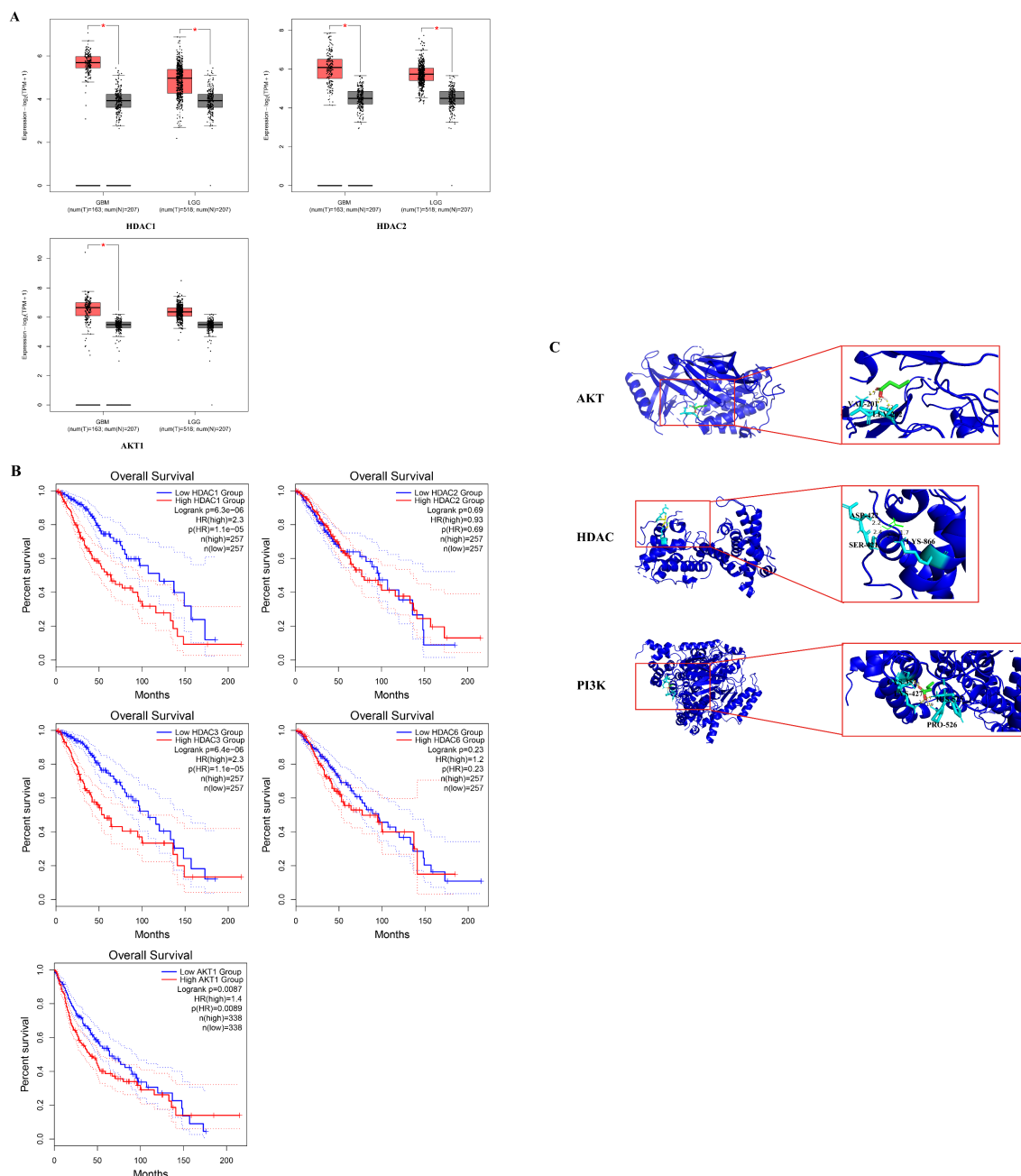


FIGURE 4 Histone Deacetylase expression upregulate in GBM clinical database and prolong glioma patients survival time. (A) The HDAC1, HDAC2 and AKT1 mRNA expression levels in common tumor tissues ($*P < 0.05$ vs. control group); (B) Overall survival of different HDAC1, HDAC2, HDAC3, HDAC6 and AKT1 level. The prognosis of the low HDAC1, HDAC3 and AKT1 expression groups was better than that of the high expression group. (C) The result diagram of molecular docking. The green 3D structural formula represents NaB; the blue bond represents the hydrogen bond at the binding site.

and glioma clinical data (Figures 2, 4), we evaluated the expression levels of class I HDACs (HDAC1, 2, 3) and class IIb HDACs (HDAC6) in U251 cells treated with sodium butyrate. The results showed that sodium butyrate significantly inhibited the expression of HDAC1, HDAC2, and HDAC3 (Figure 5C, $p < 0.01$), while the HDAC6 protein level did not change significantly (Figure 5C, $p > 0.05$).

In conclusion, our findings suggest that sodium butyrate, a class I HDAC inhibitor, induces apoptosis and cell cycle arrest in U251 cells. Additionally, it activates the PI3K/AKT pathway, which in turn upregulates PD-L1 expression in U251 cells, potentially contributing to immunological changes in the tumor microenvironment.

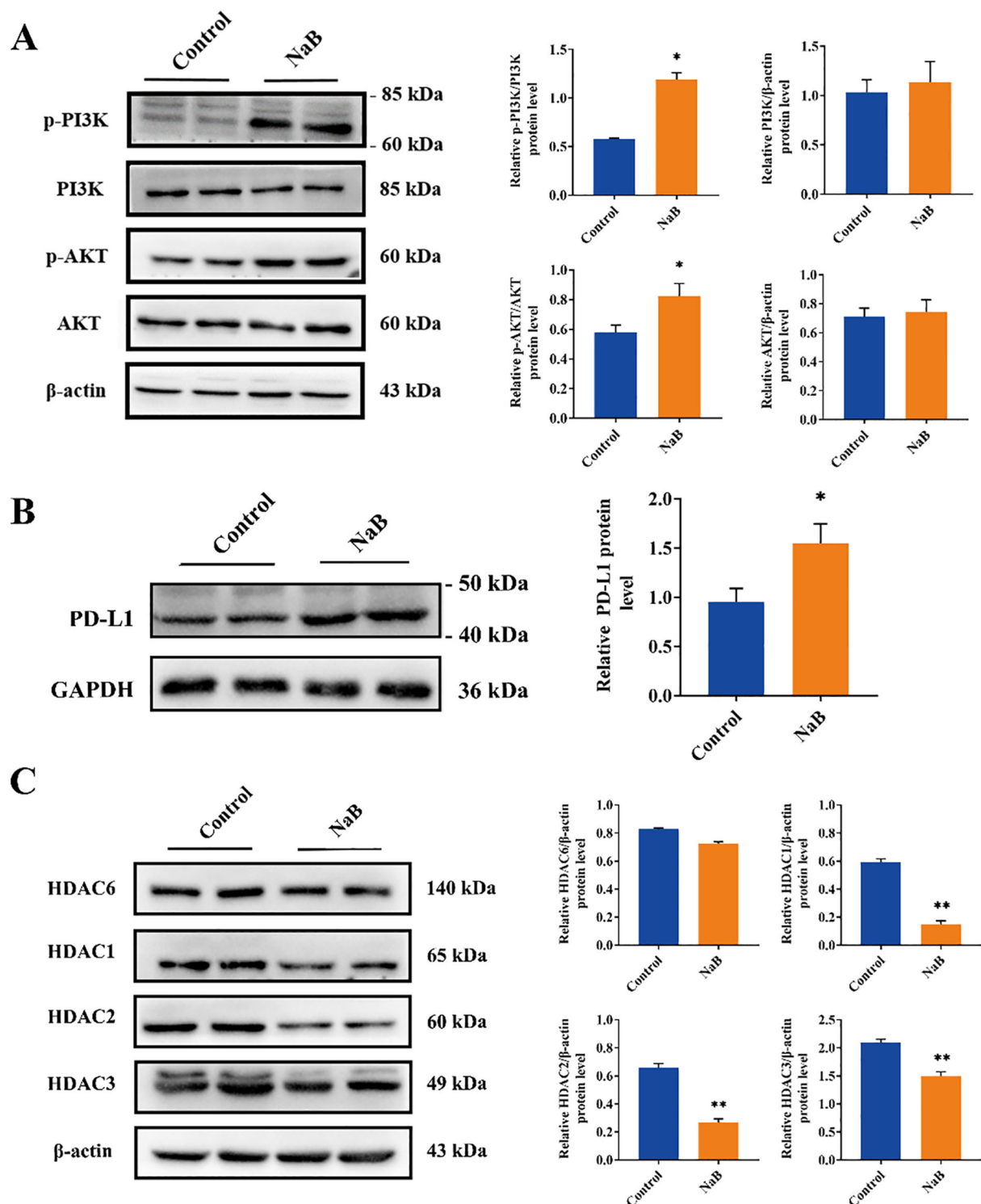


FIGURE 5

Sodium butyrate acts as a histone deacetylase inhibitor to upregulate PD-L1 protein levels in U251 cells through activation of the PI3K/AKT signaling pathway. (A–C) Representative immunoblots and quantitative analysis of the relative p-PI3K, PI3K, p-AKT, AKT, PD-L1, HDAC6, HDAC1, HDAC2, and HDAC3 protein expression in U251 cells. The data are expressed as the mean ± SEM of three independent experiments. Two-tailed, unpaired Student’s *t* test was used for statistical analysis. **p* < 0.05, ***p* < 0.01, compared with the control group.

3.6 Sodium butyrate enhanced the therapeutic effect of anti-PD-1 blockade in an orthotopic murine glioma model

Recent preclinical studies have revealed that tumor PD-L1 expression reflects an immune-active microenvironment (33), and patients with tumors expressing PD-L1 are more likely to respond to anti-PD-1 therapy (34). GBM is considered a “cold tumor” characterized by a more immunosuppressive microenvironment, with poor T-cell infiltration, high bone marrow infiltration, and low PD-L1/PD-1 expression (35, 36). In this research, to investigate whether NaB could enhance the antitumor effect of anti-PD-1 therapy *in vivo*, we tested our hypothesis using GL261 cells implanted in mice. Seven days after the implantation of GL261 cells, the tumors were treated with sodium butyrate (1.2 g/kg/d), anti-mouse PD-1 mAb alone (600 µg per mouse), or a combination of both agents (Figure 6A). Survival of glioma mice was significantly prolonged by combination therapy (median survival, 67 days) compared with treatment with NaB or an anti-mouse PD-1 mAb alone (median survival, 54.5 and 56.5 days, respectively). Treatment with sodium butyrate alone did not affect tumor growth and failed to lead to tumor regression (0/6). Treatment with anti-mouse PD-1 mAb antibodies alone effectively controlled tumor growth, and 1 out of 6 tumors were eventually cleared. However, the combination of sodium butyrate with an anti-mouse PD-1 mAb substantially slowed tumor progression and resulted in 3 complete responses out of the 6 treated mice (Figures 6B–F). These findings suggested that NaB in combination with an anti-PD-L1 antibody enhanced the antitumor effect in an orthotopic murine glioma model. To examine whether the combination therapy regulated tumor proliferation, IHC staining for Ki-67 was performed. The number of Ki-67-positive cells was lower in the combination group than in the control group (Figures 6G, H, $p < 0.01$). To evaluate the safety of the combination therapy, we performed HE staining on the liver, kidneys, and ileum and colon of the mice. HE results show that under long-term treatment, there were no morphological changes in the major metabolic organs of the glioma mice (Supplementary Figure S3). The administration of anti-PD1 in combination with sodium butyrate in glioma-bearing mice did not show significant metabolic toxicity, indicating a relatively high safety profile. In conclusion, the results of the *in vivo* study demonstrated that the combination of sodium butyrate with an anti-mouse PD-1 mAb had enhanced antitumor effects and increased survival in an orthotopic murine glioma model. This combination therapy could be a promising strategy to overcome the immunosuppressive microenvironment of glioblastoma and improve the response to anti-PD-1 therapy.

3.7 Combination therapy increases immune cytokines and T-cell infiltration in mice bearing established intracranial gliomas

We performed single-cell transcriptomic analysis on the orthotopic glioma mouse model (GSE246154) from the GEO

database using R. The results indicated that the *Ifnar2* gene was enriched in T cells (Supplementary Figures S4G, H), while the *CD68* and *CD33* genes were less enriched in macrophages (Supplementary Figure S5). T cell infiltration in the mouse glioma cells was low (Supplementary Figure S4A), further validating that glioma is a ‘cold’ tumor. The percentage of tumor-infiltrating T lymphocytes (TILs) in the four groups was assessed using flow cytometry (Figure 7A). Compared with those in the other groups, the proportions of $CD3^+CD8^+$ and $CD3^+CD4^+$ cells in the combination therapy group were significantly greater (Figure 7B, for the $CD4^+$ T cell proportion, the control group had $36.58\% \pm 4.48\%$, the PD group had $40.80\% \pm 6.34\%$, the NaB group had $37.96\% \pm 9.84\%$, and the combination group had $47.66\% \pm 4.94\%$; For the $CD8^+$ T cell proportion, the control group had $28.82\% \pm 11.07\%$, the PD group had $40.44\% \pm 8.67\%$, the NaB group had $36.08\% \pm 13.77\%$, and the combination group had $50.11\% \pm 10.53\%$). However, the percentage of Treg cells did not significantly differ between the treatment groups and the control groups (Figure 7C, $p > 0.05$). To further investigate the immune response, TILs were cultured for 4–6 hours, and the production of $IFN-\gamma$ in $CD4^+$ TILs was examined (Figure 7D). Compared with the control treatment, the combination treatment significantly increased the production of $IFN-\gamma$ by TILs (Figure 7E, $p < 0.05$). In addition, CD4 and CD8 positive cells were characterized in the tumor tissue using immunohistochemical analysis. The combination therapy group exhibited a substantial increase in the number of CD8 and CD4 positive cells (Figure 7F, $p < 0.001$), which was consistent with the flow cytometry results. Moreover, the $CD8^+$ T-cell number was also significantly greater in the anti-mouse PD-1 group than in the control group (Figure 7G, $p < 0.05$). Overall, the results indicate that the combination of sodium butyrate with an anti-mouse PD-1 antibody effectively retards tumor growth and enhances the antitumor response by promoting and optimizing the tumor microenvironment. This combination therapy appears to induce a more immune-active microenvironment, with increased TILs, elevated $CD4^+$ and $CD8^+$ T-cell ratios, and enhanced $IFN-\gamma$ production, ultimately contributing to the antitumor effects observed.

3.8 Effects of sodium butyrate and PD-1 inhibitor administration on the gut microbiota and its metabolites in glioma mice

Notably, glioma growth has been reported to induce changes in fecal SFCA levels and neurotransmitters (37, 38). In the present study, LC-MS/MS analysis revealed a significant decrease in fecal sodium butyrate content in tumor-bearing mice compared to pre-tumor implantation levels (Figure 8A).

We also examined changes in the gut microbiota composition among the four treatment groups using 16S rRNA sequencing. The α -diversity of the gut microbiota was assessed using four different metrics. The results showed that the combination therapy of sodium butyrate with anti-mouse PD-1 did not significantly affect the α -

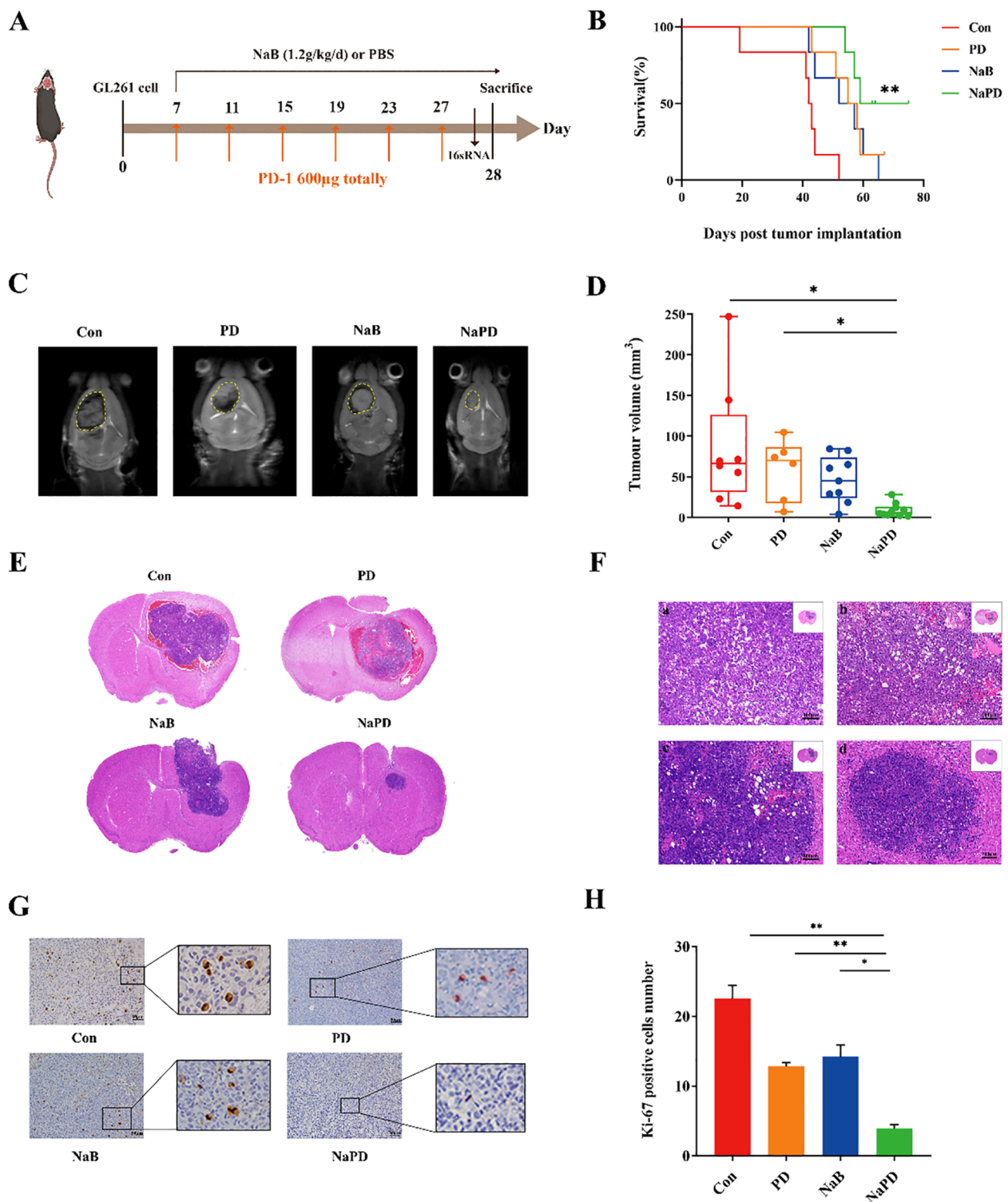
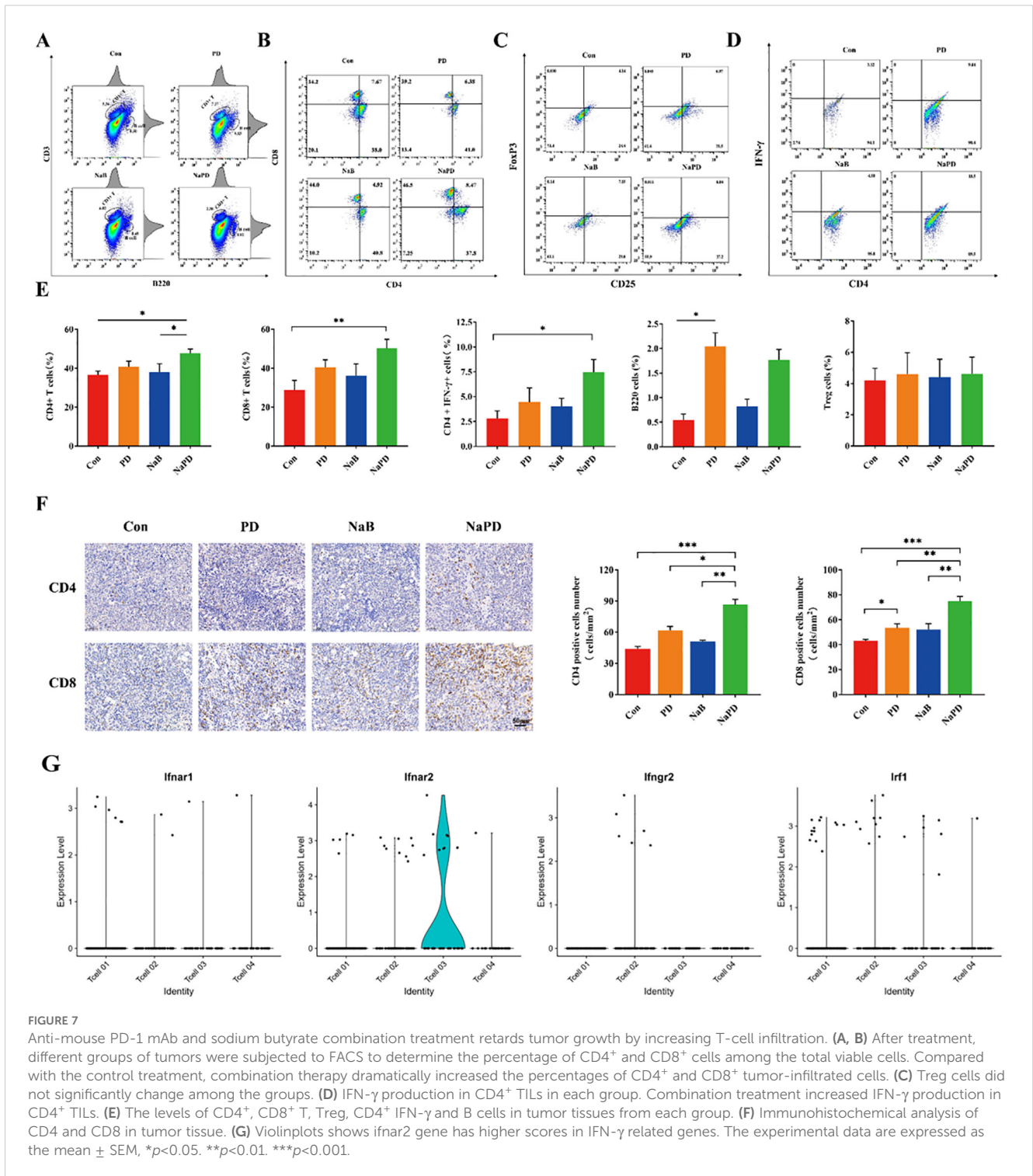


FIGURE 6

Combinatorial therapy with anti-mouse PD-1 mAb and sodium butyrate in an orthotopic murine glioma model. GL261 glioma cells were implanted into C57BL/6 mice. Seven days after inoculation, the mice were treated with NaB (1.2 g/kg/d), an anti-mouse PD-1 mAb (600 µg), a combination of the two reagents, or a solvent control as indicated (A). K–M survival curves (B) were generated to evaluate glioma mouse survival time, n = 6, log-rank test. Compared with Con group, $**p < 0.01$, NS not show. The tumor volumes of the mice were measured with MRI after drug treatment for 21 days (C), and the tumor volumes (D) were calculated. Compared with the Con and PD group, $*p < 0.05$, NS not show. (E, F) Tumor sections were prepared and stained with H&E for histological examination ($\times 100$). Moreover, representative Ki-67-stained sections ($\times 200$, G) and the numbers of Ki-67-positive cells in brain tissues (H) are shown. The experimental data are expressed as the mean \pm SEM. Compared with the control and PD groups, $**p < 0.01$. Compared with the NaB group, $*p < 0.05$.



diversity of the gut microbiota in glioma-bearing mice (Figure 8B). However, β diversity analysis (PCoA) demonstrated that the gut microbiota in the combination group was more similar to that of the anti-mouse PD-1 group, and more distinct from that of the NaB group (Figure 8C). The gut microbiota in the four groups was dominated by *Bacteroidetes* and *Firmicutes* at the phylum level, and significant changes in each group were not observed (data not shown). Interestingly, genus-level analysis revealed that the top-

ranked genera were *Lachnospiraceae_NK4A136_group*, *Lactobacillus* and *Helicobacter* (Figure 8D). *Lactobacillus* is a recognized probiotic and is often used as a fermenting agent in yogurt (39). Compared to that in the control group, the relative abundance of *Lactobacillus* was significantly greater in the combination group ($p < 0.05$). *Lachnospiraceae_NK4A136_group* was one of the genera that produces SCFAs (40); however, there was no difference among the groups of mice ($p > 0.05$), indicating that

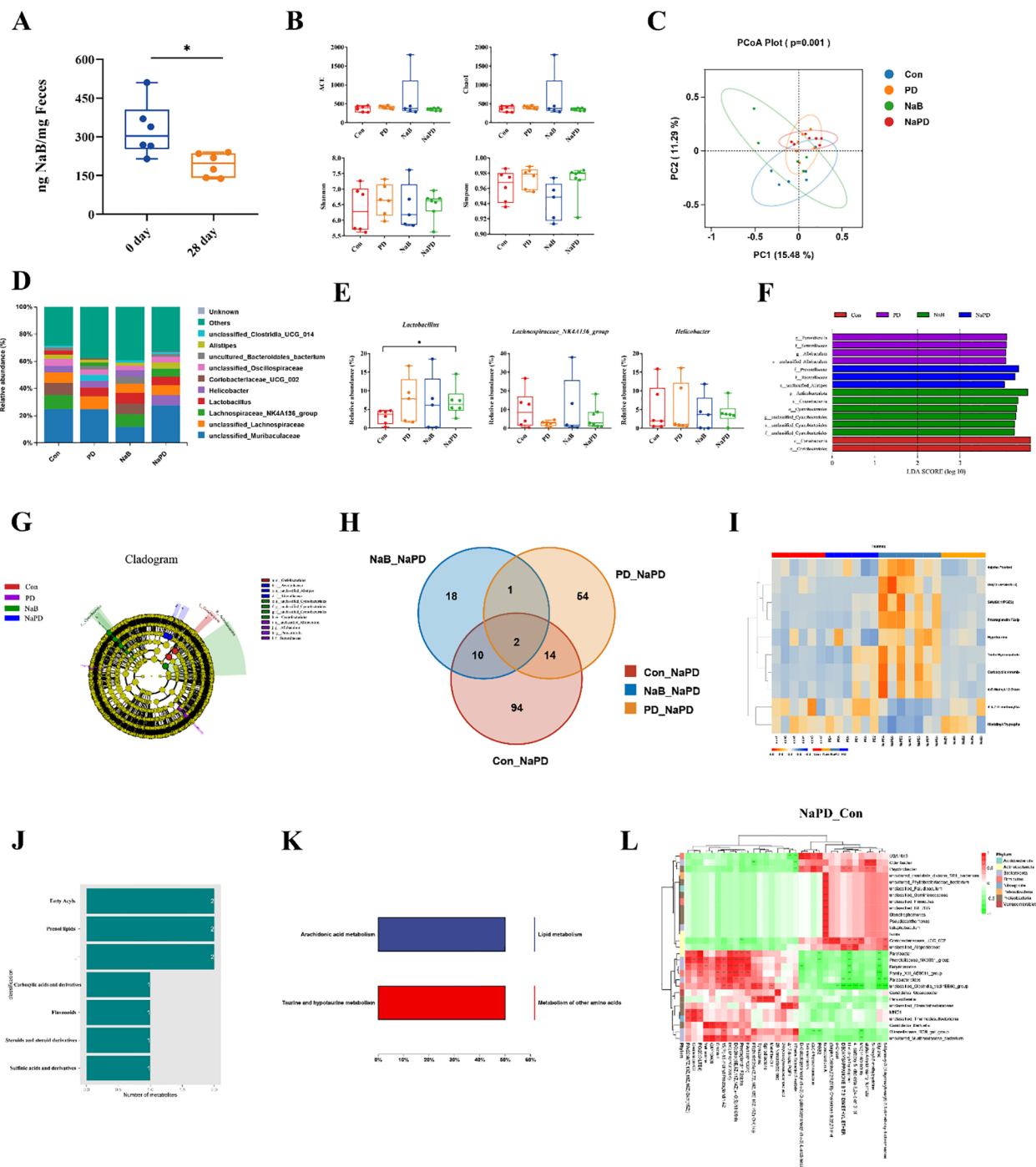


FIGURE 8 Combined analysis of the gut microbiota and its metabolites in glioma mice. **(A)** NaB content in the feces of mice before and after glioma implantation. The data are expressed as the mean \pm SD, $n = 6$. $*p < 0.05$. Changes in the gut microbiota diversity of different groups, **(B)** ACE, Chao1, Shannon and Simpson indices. **(C)** PCoA analysis of gut microbiota β diversity. **(D)** Species distribution map of the gut microbiota at the genus level. **(E)** Relative abundances of *Lactobacillus*, *Lachnospiraceae_NK4A136_group* and *Helicobacter*. The experimental data are expressed as 5 - 95% confidence intervals, $n = 5-6$. Compared with the model group. $*p < 0.05$. **(F, G)** LefSe analysis of the gut microbiota in different groups. **(H)** Venn diagram of the differentially abundant metabolites between the NaPD and Con groups and between the PD group and the NaB group. **(I-K)** Classification of differentially abundant metabolites in the combination group and their functional analysis. **(L)** Differentially abundant metabolite clustering-microbial correlation analysis for the combination group (genus level).

exogenous administration of NaB had no significant effect on the abundance of SCFA-producing microbiota. *Helicobacter* is a pathogenic bacteria (41), and the relative abundance of *Helicobacter* did not differ significantly among the four groups of mice ($p > 0.05$), suggesting that *Helicobacter* abundance was not significantly associated with glioma treatment (Figure 8E). In the combination group, *Bacteroides* was enriched (*f:Rikenellaceae, f:Prevotellaceae, s:unclassified_Alistipes*, Figures 8F, G).

The untargeted metabolomics analysis by GC-MS revealed 10 shared differentially abundant metabolites in the combination group compared to the other three groups, suggesting their specificity in the combination group (Figure 8H). We annotated the 10 shared differentially abundant metabolites, and the results are shown in Figure 8I. The shared differentially abundant metabolites in the combination group were fatty acyls, prenol lipids, carboxylic acids and derivatives, flavonoids, steroids and steroid derivatives, and sulfonic acids and derivatives (Figure 8J). To investigate the function of the differentially abundant metabolites in the combination group, we performed KEGG enrichment analysis, and the results showed that the differentially abundant metabolites were mainly involved in lipid metabolism and other amino acid metabolism (Figure 8K).

Further correlation analysis was performed between the differentially abundant metabolites and the differential flora at the genus level. The heatmap shows the magnitude and direction of correlation between various differentially abundant metabolites and each differential flora classification (Figure 8L). Significant correlations ($p < 0.05$) between metabolite clusters and microorganisms were observed, indicating potential interactions between specific gut microbial communities and metabolites in the combination group.

These results collectively indicate that the combination of sodium butyrate with an anti-mouse PD-1 antibody affects the gut microbiota composition and metabolic profiles in glioma-bearing mice. The alterations in the gut microbiota and associated metabolites might contribute to the observed enhanced antitumor effects and improved tumor microenvironment in response to the combination therapy.

4 Discussion

In our work, we experimentally investigated the role of sodium butyrate in glioma cells and its combination with a PD-1 inhibitor in a glioma mouse model. Sodium butyrate, as one of the gut microbiota metabolites, upregulates PD-L1 expression in glioma cells by regulating the PI3K/AKT pathway, helping to transform GBM cells from a “cold tumor” to a “hot tumor”, and improving the efficacy of PD-1 inhibitors for GBM treatment. Single-cell data analysis indicates that glioma-bearing mice have a low proportion of T cells, classifying glioma as a “cold tumor.” Additionally, IFN γ related genes enrichment are minimal. The combination therapy promoted tumor immune cell infiltration, prolonged the survival time of glioma-bearing mice and inhibited glioma growth. Since sodium butyrate (NaB) is a nontoxic four-carbon short-chain fatty acid produced during the fermentation of dietary fiber in the colon and is a natural inhibitor of histone deacetylase, we demonstrated

that glioma growth decreases the NaB content in the feces. Furthermore, combination therapy increases the proportion of probiotics in the gut microbiota of tumor-bearing mice, promotes antitumor metabolites and decreases metabolites that affect immune cell function, thus inhibiting the growth of gliomas in mice through the “brain-gut axis”.

Histone acetylations are a key component of epigenetics, and inhibition of histone deacetylases induces acute hyperacetylation of epigenetic regulators at the histone-chromatin interface, resulting in the regulation of RNA polymerase II (Pol II)-driven transcription (42). In cancer cells, this regulation of transcription includes tumor suppression, antigen processing and expression mechanisms, and re-expression of tumor antigen-associated genes (30, 43). NaB is a natural histone deacetylase inhibitor (44). To investigate the effect of NaB on glioma cells, we first examined the proliferation of NaB-treated U251 cells using a CCK-8 assay, and the results showed that treatment of glioma cells with 7 mM NaB for 48 h significantly inhibited glioma cell proliferation. Second, Annexin V/PI double staining showed that NaB significantly induced apoptosis in glioma cells. qPCR and WB results showed that NaB downregulated Survivin protein levels in glioma cells. Finally, PI staining flow cytometry, qPCR and WB showed that NaB blocked the cell cycle of glioma cells by downregulating CDC2, CDC25C, CCNA2 and CCNB cell cycle-related proteins. The above results suggest that NaB, an HDACi, can inhibit the growth of glioma cells.

Both abnormally upregulated PD-L1 expression and a lack of PD-L1 led to ineffective PD-1/PD-L1 inhibitors. However, the expression of PD-L1 or PD-1 is a prerequisite for therapeutic efficacy. In prostate cancer, low PD-L1 expression is associated with a poorer PD-1 blockade response (24). We used RNA-seq to detect DEGs in NaB-treated U251 cells. KEGG enrichment analysis revealed that the upregulated genes were enriched mainly in cancer-related signaling pathways, and GSEA further revealed that the upregulated genes were involved in immune-related systems. GSEA further revealed that the upregulated genes were enriched mainly in PD-1/PD-L1 immune checkpoints. To verify the accuracy of the sequencing results, we examined the PD-L1 protein levels in NaB-treated U251 cells by Western blot and found that NaB significantly upregulated PD-L1 protein expression in U251 cells compared to that in the control group, which was consistent with the transcriptome sequencing results.

PD-L1 transcript levels are regulated by multiple signaling pathways, and our differential gene set enrichment analysis (GSEA) revealed that among the signaling pathway-related gene clusters, upregulated genes were enriched in the PI3K/AKT pathway. The next experiment also demonstrated that NaB activates the PI3K/AKT pathway in glioma cells, as evidenced by the significant upregulation of p-PI3K and p-AKT (Figure 5A). Activation of the PI3K pathway has been reported to lead to increased PD-L1 expression in glioma cells (17). IFN γ mediates the activation of the AKT-mTOR signaling pathway in non-small cell lung cancer, increasing its PD-L1 expression (45). Similarly, activation of the MAPK and PI3K pathways in melanoma also upregulates PD-L1 expression (46). This finding is consistent with our experimental results, both suggesting that the PI3K/AKT

signaling pathway plays an important role in regulating PD-L1 transcript levels. Furthermore, there are other signaling pathways that regulate PD-L1 expression, such as in lung cancer cells, where PD-L1 expression may be regulated by the epidermal growth factor receptor (EGFR) pathway (47). In T-cell lymphoma, STAT3 silencing reduces PD-L1 expression (48). In breast cancer, reactive oxygen species (ROS) accumulation activates the downstream NF- κ B signaling pathway, which increases PD-L1 protein levels (49). However, whether NaB mediates PD-L1 expression by regulating other signaling pathways and how NaB, as an HDACi, activates the PI3K/AKT signaling pathway in glioma cells in terms of epistasis modification need further investigation.

Since NaB is mainly metabolized by the gut microbiota *in vivo*, we performed a combined analysis of microorganisms and their metabolites in the feces of each group of mice. 16S RNA sequencing revealed no significant differences between the different groups at the phylum level and no significant changes in the *Firmicutes*, *Bacteroidetes* or F/B ratio. At the genus level, the abundance of *Lactobacillus* was significantly greater in the combination group than in the control group. *Lactobacillus* is a recognized probiotic and has potential anticancer effects. *Lactobacillus* can interact with proteins that regulate the cell cycle and inhibit the proliferation of cancer cells (39). Researchers found that a gavage mixture of *Lactobacillus* and *Bifidobacterium* inhibited the growth of brain gliomas in mice (50). We therefore hypothesized that the combination therapy was able to increase the abundance of probiotics in the gut microbiota of mice to promote the therapeutic effect on glioma. *Lachnospiraceae_NK4A136_group* is a genus that produces SCFAs. However, there was no difference among the groups of mice ($p > 0.05$), indicating that exogenous administration of NaB had no significant effect on the abundance of SCFA-producing microbiota. The effect of the gut microbiota on the organism acts mainly through its metabolites, and we used LC-MS to measure the changes in metabolites of the gut microbiota in each group. We found that the top three upregulated metabolites that differed between the combination and control groups were statins, ethyladipic acid and N-methylphenylethanolamine. The three most downregulated metabolites were 4-O-methylgalactinol, 2-isopropyl-1,4-hexadiene and methyl linoleate. In addition to their cholesterol-lowering effects (51), statins have proapoptotic, antiangiogenic, and immunomodulatory effects. Statins have been shown to inhibit the growth of several cancer cell types, such as neuroblastoma, breast cancer, melanoma, and acute myeloid leukemia cells (52). Therefore, we speculate that the better therapeutic effect of NaB in combination with a PD-1 inhibitor in glioma may be related to the increase in active antitumor substances in the metabolites of the gut microbiota and the decrease in substances that inhibit the function of T cells.

Taken together, our study demonstrates that glioma growth reduces the levels of microbiome-derived sodium butyrate in mice. Sodium butyrate inhibits glioma cell growth *in vitro*, arrests the cell cycle, and enhances PD-L1 expression in glioma cells by activating the PI3K/AKT pathway, which may facilitate the conversion of gliomas from 'cold' tumors to 'hot' tumors. In an orthotopic glioma mouse model, sodium butyrate enhances the efficacy of anti-PD-1 immunotherapy by modulating the immune infiltration of cytotoxic CD8⁺ T cells. These

findings suggest that sodium butyrate is a promising biomarker that could significantly improve the therapeutic outcomes for glioma patients.

5 Conclusions

First, sodium butyrate significantly inhibited the viability of U251 and GL261 glioma cells, with U251 cells showing higher sensitivity. Flow cytometry indicated an increased percentage of apoptotic U251 cells after 48 hours of NaB treatment. NaB also reduced survivin mRNA and protein levels in U251 cells.

Besides, RNA-seq analysis revealed significant changes in gene expression related to the cell cycle, PD-L1 expression, and the PI3K/Akt pathway after NaB treatment. NaB downregulated CDC2 and other cell cycle-related proteins, activated the PI3K/AKT pathway, and increased PD-L1 expression on the cell surface. NaB also inhibited HDAC1 expression. Moreover, analysis of a glioblastoma multiforme (GBM) clinical database indicated that lower expressions of HDAC1, HDAC3, and AKT1 correlated with better overall survival in glioma patients. Molecular docking studies showed that NaB could bind well to AKT1, PI3K, and HDAC proteins. In a mouse glioma model, the combination of NaB and a PD-1 inhibitor significantly reduced tumor size and extended survival. This combination therapy increased immune cytokines and T-cell infiltration in glioma-bearing mice. Last, NaB also act as a major metabolite of the gut microbiota, altered the gut microbiota composition and metabolic profiles in glioma mice, enhancing the antitumor effects and improving the tumor microenvironment.

Overall, this study is the first to discover that the combination of sodium butyrate with an anti-PD-1 antibody demonstrates significant potential in treating gliomas by modulating immune responses and affecting gut microbiota, providing insights into overcoming the limitations of current glioma clinical treatments.

Data availability statement

The data presented in the study are deposited in the NCBI repository, accession number PRJNA1243548 and PRJNA1243480.

Ethics statement

The animal study was approved by Medical Ethics Committee of Sichuan University. The study was conducted in accordance with the local legislation and institutional requirements.

Author contributions

SL: Data curation, Investigation, Methodology, Software, Writing – original draft. LW: Formal Analysis, Methodology, Writing – original draft. MH: Data curation, Project administration, Writing – original draft. HF: Supervision, Writing – original draft. HT: Supervision,

Writing – review & editing. HG: Resources, Writing – review & editing. GL: Resources, Writing – review & editing. ZX: Resources, Writing – review & editing. CP: Resources, Writing – review & editing. JD: Resources, Writing – review & editing. ZZ: Resources, Writing – review & editing. FP: Funding acquisition, Project administration, Resources, Supervision, Writing – review & editing.

Funding

The author(s) declare that financial support was received for the research and/or publication of this article. The study was supported by National Natural Science Foundation of Science and Technology Department of Sichuan Province (no.2023NSFSC1928), Project of State Administration of Traditional Chinese Medicine of China (no.ZYYCXTD-D-202209), Project of Sichuan Provincial Administration of Traditional Chinese Medicine (no.2022C001) and the Open Research Fund of State Key Laboratory of Southwestern Chinese Medicine Resources (no.SKLTTCM202404).

Conflict of interest

Author LW was employed by the company Jiangsu Sanshu Biotechnology Co., Ltd.

References

- Ostrom QT, Gittleman H, Truitt G, Boscia A, Kruchko C, Barnholtz-Sloan JS. CBTRUS statistical report: primary brain and other central nervous system tumors diagnosed in the United States in 2011–2015. *Neuro-Oncology*. (2018) 20:iv1–iv86. doi: 10.1093/neuonc/ny131
- Zhou Y, Zhou B, Pache L, Chang M, Khodabakhshi AH, Tanaseichuk O, et al. Metascape provides a biologist-oriented resource for the analysis of systems-level datasets. *Nat Commun*. (2019) 10:1523. doi: 10.1038/s41467-019-09234-6
- Li BH, Rao LP. Pump proton inhibitors display anti-tumour potential in glioma. *Cell Proliferation*. (2023) 56(7). doi: 10.1111/cpr.13321
- Taube JM, Anders RA, Young GD, Xu H, Sharma R, McMiller TL, et al. Colocalization of inflammatory response with B7-h1 expression in human melanocytic lesions supports an adaptive resistance mechanism of immune escape. *Sci Transl Med*. (2012) 4:127ra37. doi: 10.1126/scitranslmed.3003689
- Goswami S, Walle T, Cornish AE, Basu S, Anandhan S, Fernandez I, et al. Immune profiling of human tumors identifies CD73 as a combinatorial target in glioblastoma. *Nat Med*. (2020) 26:39–46. doi: 10.1038/s41591-019-0694-x
- Iglesia MD, Parker JS, Hoadley KA, Serody JS, Perou CM, Vincent BG. Genomic analysis of immune cell infiltrates across 11 tumor types. *J Natl Cancer Inst*. (2016) 108(11). doi: 10.1093/jnci/djw144
- Nduom EK, Wei J, Yaghi NK, Huang N, Kong LY, Gabrusiewicz K, et al. PD-L1 expression and prognostic impact in glioblastoma. *Neuro Oncol*. (2016) 18:195–205. doi: 10.1093/neuonc/nov172
- Filley AC, Henriquez M, Dey M. Recurrent glioma clinical trial, CheckMate-143: the game is not over yet. *Oncotarget*. (2017) 8:91779–94. doi: 10.18632/oncotarget.21586
- Routy B, Le Chatelier E, Derosa L, Duong CPM, Alou MT, Daillère R, et al. Gut microbiome influences efficacy of PD-1-based immunotherapy against epithelial tumors. *Science*. (2018) 359:91–7. doi: 10.1126/science.aan3706
- Lu Y, Yuan X, Wang M, He Z, Li H, Wang J, et al. Gut microbiota influence immunotherapy responses: mechanisms and therapeutic strategies. *J Hematol Oncol*. (2022) 15:47. doi: 10.1186/s13045-022-01273-9
- Wang L, Tang L, Zhai D, Song M, Li W, Xu S, et al. The role of the sex hormone-gut microbiome axis in tumor immunotherapy. *Gut Microbes*. (2023) 15:2185035. doi: 10.1080/19490976.2023.2185035
- Zitvogel L, Ma Y, Raouf D, Kroemer G, Gajewski TF. The microbiome in cancer immunotherapy: Diagnostic tools and therapeutic strategies. *Science*. (2018) 359:1366–70. doi: 10.1126/science.aar6918
- Baruch EN, Wang J, Wargo JA. Gut microbiota and antitumor immunity: potential mechanisms for clinical effect. *Cancer Immunol Res*. (2021) 9:365–70. doi: 10.1158/2326-6066.CIR-20-0877
- Yang X, Yu D, Xue L, Li H, Du J. Probiotics modulate the microbiota-gut-brain axis and improve memory deficits in aged SAMP8 mice. *Acta Pharm Sin B*. (2020) 10:475–87. doi: 10.1016/j.apsb.2019.07.001
- He Z, Wang M, Li H, Wen C. GC-MS-based fecal metabolomics reveals gender-attributed fecal signatures in ankylosing spondylitis. *Sci Rep*. (2019) 9:3872. doi: 10.1038/s41598-019-40351-w
- Shojaei F, Yazdani-Nafchi F, Banitalebi-Dehkordi M, Chehelgerdi M, Khorramian-Ghahfarokhi M. Trace of survivin in cancer. *Eur J Cancer Prev*. (2019) 28:365–72. doi: 10.1097/CEJ.00000000000000453
- Parsa AT, Waldron JS, Panner A, Crane CA, Parney IF, Barry JJ, et al. Loss of tumor suppressor PTEN function increases B7-H1 expression and immunoresistance in glioma. *Nat Med*. (2007) 13:84–8. doi: 10.1038/nm1517
- Dorée M, Hunt T. From Cdc2 to Cdk1: when did the cell cycle kinase join its cyclin partner? *J Cell Sci*. (2002) 115:2461–4. doi: 10.1242/jcs.115.12.2461
- Coffman JA. Cell cycle development. *Dev Cell*. (2004) 6:321–7. doi: 10.1016/S1534-5807(04)00067-X
- Liu K, Zheng M, Lu R, Du J, Zhao Q, Li Z, et al. The role of CDC25C in cell cycle regulation and clinical cancer therapy: a systematic review. *Cancer Cell Int*. (2020) 20:213. doi: 10.1186/s12935-020-01304-w
- Dumitru AMG, Compton DA. Identifying cyclin A/Cdk1 substrates in mitosis in human cells. *Methods Mol Biol*. (2022) 2415:175–82. doi: 10.1007/978-1-0716-1904-9_13
- Jin M, Li J, Hu R, Xu B, Huang G, Huang W, et al. Cyclin A2/cyclin-dependent kinase 1-dependent phosphorylation of Top2a is required for S phase entry during retinal development in zebrafish. *J Genet Genomics*. (2021) 48:63–74. doi: 10.1016/j.jgg.2021.01.001
- Han Y, Liu D, Li L. PD-1/PD-L1 pathway: current researches in cancer. *Am J Cancer Res*. (2020) 10:727–42.

The remaining authors declare that the research was conducted in the absence of any commercial or financial relationships that could be construed as potential conflicts of interest.

Generative AI statement

The author(s) declare that no Generative AI was used in the creation of this manuscript.

Publisher's note

All claims expressed in this article are solely those of the authors and do not necessarily represent those of their affiliated organizations, or those of the publisher, the editors and the reviewers. Any product that may be evaluated in this article, or claim that may be made by its manufacturer, is not guaranteed or endorsed by the publisher.

Supplementary material

The Supplementary Material for this article can be found online at: <https://www.frontiersin.org/articles/10.3389/fimmu.2025.1532528/full#supplementary-material>

24. Zou W, Chen L. Inhibitory B7-family molecules in the tumour microenvironment. *Nat Rev Immunol.* (2008) 8:467–77. doi: 10.1038/nri2326
25. Wu B, Song M, Dong Q, Xiang G, Li J, Ma X, et al. UBR5 promotes tumor immune evasion through enhancing IFN- γ -induced PDL1 transcription in triple negative breast cancer. *Theranostics.* (2022) 12:5086–102. doi: 10.7150/thno.74989
26. Lamichhane P, Karyampudi L, Shreeder B, Krempsi J, Bahr D, Daum J, et al. IL10 release upon PD-1 blockade sustains immunosuppression in ovarian cancer. *Cancer Res.* (2017) 77:6667–78. doi: 10.1158/0008-5472.CAN-17-0740
27. Atsaves V, Tsesmetzis N, Chioureas D, Kis L, Leventaki V, Drakos E, et al. PD-L1 is commonly expressed and transcriptionally regulated by STAT3 and MYC in ALK-negative anaplastic large-cell lymphoma. *Leukemia.* (2017) 31:1633–7. doi: 10.1038/leu.2017.103
28. Casey SC, Tong L, Li Y, Do R, Walz S, Fitzgerald KN, et al. MYC regulates the antitumor immune response through CD47 and PD-L1. *Science.* (2016) 352:227–31. doi: 10.1126/science.aac9935
29. Bu LL, Yu GT, Wu L, Mao L, Deng WW, Liu JF, et al. STAT3 induces immunosuppression by upregulating PD-1/PD-L1 in HNSCC. *J Dent Res.* (2017) 96:1027–34. doi: 10.1177/002203451712435
30. West AC, Johnstone RW. New and emerging HDAC inhibitors for cancer treatment. *J Clin Invest.* (2014) 124:30–9. doi: 10.1172/JCI69738
31. Topper MJ, Vaz M, Marrone KA, Brahmner JR, Baylin SB. The emerging role of epigenetic therapeutics in immuno-oncology. *Nat Rev Clin Oncol.* (2020) 17:75–90. doi: 10.1038/s41571-019-0266-5
32. Bridgeman S, Woo HC, Newsholme P, Mamotte C. Butyrate lowers cellular cholesterol through HDAC inhibition and impaired SREBP-2 signalling. *Int J Mol Sci.* (2022) 23(4). doi: 10.3390/ijms232415506
33. Taube JM, Klein A, Brahmner JR, Xu H, Pan X, Kim JH, et al. Association of PD-1, PD-1 ligands, and other features of the tumor immune microenvironment with response to anti-PD-1 therapy. *Clin Cancer Res.* (2014) 20(19):5064–74. doi: 10.1158/1078-0432.CCR-13-3271
34. Tumeh PC, Harville CL, Yearley JH, Shintaku IP, Taylor EJ, Robert L, et al. PD-1 blockade induces responses by inhibiting adaptive immune resistance. *Nature.* (2014) 515:568–71. doi: 10.1038/nature13954
35. Quail DF, Joyce JA. The microenvironmental landscape of brain tumors. *Cancer Cell.* (2017) 31:326–41. doi: 10.1016/j.ccell.2017.02.009
36. Chuntova P, Chow F, Watchmaker PB, Galvez M, Heimberger AB, Newell EW, et al. Unique challenges for glioblastoma immunotherapy—discussions across neuro-oncology and non-neuro-oncology experts in cancer immunology. Meeting Report from the 2019 SNO Immuno-Oncology Think Tank. *Neuro Oncol.* (2021) 23:356–75. doi: 10.1093/neuonc/noaa277
37. Dono A, Patrizzi A, McCormack RM, Putluri N, Ganesh BP, Kaur B, et al. Glioma induced alterations in fecal short-chain fatty acids and neurotransmitters. *CNS Oncol.* (2020) 9:Cns57. doi: 10.2217/cns-2020-0007
38. Han M, Li S, Fan H, An J, Peng C, Peng F. Regulated cell death in glioma: promising targets for natural small-molecule compounds. *Front Oncol.* (2024) 14:1273841. doi: 10.3389/fonc.2024.1273841
39. Nowak A, Paliwoda A, Blasiak J. Anti-proliferative, pro-apoptotic and anti-oxidative activity of Lactobacillus and Bifidobacterium strains: A review of mechanisms and therapeutic perspectives. *Crit Rev Food Sci Nutr.* (2019) 59:3456–67. doi: 10.1080/10408398.2018.1494539
40. Zou YT, Zhou J, Zhu JH, Wu CY, Shen H, Zhang W, et al. Gut microbiota mediates the protective effects of traditional Chinese medicine formula Qiong-Yu-Gao against cisplatin-induced acute kidney injury. *Microbiol Spectr.* (2022) 10:e0075922. doi: 10.1128/spectrum.00759-22
41. Mladenova-Hristova I, Grekova O, Patel A. Zoonotic potential of Helicobacter spp. *J Microbiol Immunol Infect.* (2017) 50:265–9. doi: 10.1016/j.jmii.2016.11.003
42. Shvedunova M, Akhtar A. Modulation of cellular processes by histone and non-histone protein acetylation. *Nat Rev Mol Cell Biol.* (2022) 23:329–49. doi: 10.1038/s41580-021-00441-y
43. Wang YH, An JS, Zhou JB, Chang LM, Zhang Q, Peng F. Hydroxysafflor yellow A: a natural pigment with potential anticancer therapeutic effect. *Front In Pharmacol.* (2025) 15. doi: 10.3389/fphar.2024.1495393
44. Davie JR. Inhibition of histone deacetylase activity by butyrate. *J Nutr.* (2003) 133:2485s–93s. doi: 10.1093/jn/133.7.2485S
45. Lastwika KJ, Wilson W 3rd, Li QK, Norris J, Xu H, Ghazarian SR, et al. Control of PD-L1 expression by oncogenic activation of the AKT-mTOR pathway in non-small cell lung cancer. *Cancer Res.* (2016) 76:227–38. doi: 10.1158/0008-5472.CAN-14-3362
46. Atefi M, Avramis E, Lassen A, Wong DJ, Robert L, Foulad D, et al. Effects of MAPK and PI3K pathways on PD-L1 expression in melanoma. *Clin Cancer Res.* (2014) 20:3446–57. doi: 10.1158/1078-0432.CCR-13-2797
47. Akbay EA, Koyama S, Carretero J, Altabel A, Tchaicha JH, Christensen CL, et al. Activation of the PD-1 pathway contributes to immune escape in EGFR-driven lung tumors. *Cancer Discovery.* (2013) 3:1355–63. doi: 10.1158/2159-8290.Cd-13-0310
48. Song TL, Nairismägi ML, Laurensia Y, Lim JQ, Tan J, Li ZM, et al. Oncogenic activation of the STAT3 pathway drives PD-L1 expression in natural killer/T-cell lymphoma. *Blood.* (2018) 132:1146–58. doi: 10.1182/blood-2018-01-829424
49. Roux C, Jafari SM, Shinde R, Duncan G, Cescon DW, Silvester J, et al. Reactive oxygen species modulate macrophage immunosuppressive phenotype through the up-regulation of PD-L1. *Proc Natl Acad Sci U S A.* (2019) 116:4326–35. doi: 10.1073/pnas.1819473116
50. Wang L, Li S, Fan H, Han M, Xie J, Du J, et al. Bifidobacterium lactis combined with Lactobacillus plantarum inhibit glioma growth in mice through modulating PI3K/AKT pathway and gut microbiota. *Front Microbiol.* (2022) 13:986837. doi: 10.3389/fmicb.2022.986837
51. Sirtori CR. The pharmacology of statins. *Pharmacol Res.* (2014) 88:3–11. doi: 10.1016/j.phrs.2014.03.002
52. Vallianou NG, Kostantinou A, Kougias M, Kazazis C. Statins and cancer. *Anticancer Agents Med Chem.* (2014) 14:706–12. doi: 10.2174/1871520613666131129105035

Glossary

ALT	Alanine aminotransferase	lncRNAs	long noncoding RNA
AST	Aspartate aminotransferase	MRI	Magnetic resonance imaging
BUN	Blood urea nitrogen	NaB	Sodium butyrate
CCNA2	Cyclin A2	OS	Overall Survival
CCNB1	Cyclin B12	PAGE	Polyacrylamide gel electrophoresis
CDK	Cyclin-dependent kinases	PBS	Phosphate buffered saline
CRE	Creatinine	PD-1	Programmed cell death-1
CTLA-4	Cytotoxic T-lymphocyte-associated protein 4	PD-L1	Programmed cell death 1 ligand 1
DAB	3,3'-diaminobenzidine	PFS	progression-free survival
DEPC	Diethylpyrocarbonate	PI	Propidium
DMEM	Dulbecco's modified eagle medium	PI3K	Phosphatidylinositol 3-kinase
ECL	Enhanced chemiluminescence	PMSF	Phenylmethanesulfonyl fluoride
ES	Enrichment score	Pol II	RNA polymerase II
FDA	Food and drug administration	PVDF	Polyvinylidene fluoride
GC-MS	Gas chromatograph-mass spectrometry	qPCR	Real-time quantitative polymerase chain reaction
GFAP	Glial fibrillary acidic protein	SCFA	Short chain fatty acid
GBM	Glioblastoma	SDS	Sodium dodecyl sulfate
GO	Gene ontology	SRS	Stereotactic radiosurgery
GSEA	Gene Set Enrichment Analysis	STAT3	Signal transducer and activator of transcription
HDAC	Histone deacetylase	T2WI	T2 weighted imaging
HGG	High-grade glioma	TIM-3	T cell immunoglobulin-3
HMDB	Human metabolome database	TILs	Tumor-infiltrating lymphocytes
ICI	Immune checkpoint inhibitors	TME	Tumor microenvironment
IFN	Interferon	TMZ	Temozolomide
IHC	Immunohistochemistry	Treg	Regulatory T-cells
JAK	Janus kinase	TTF	tumor treating fields
KEGG	Kyoto encyclopedia of genes and genomes	VIP	Variable importance in the projection
LC-MS	Liquid chromatograph-mass spectrometry	WHO	World health organization
LEfSe	Linear discriminant analysis Effect Size		